

QWIP & T2SL Detectors for Space Applications.

Lukas Welzel

Leiden Observatory, Leiden University
e-mail: welzel@strw.leidenuniv.nl

March 28, 2023

Key words. infrared detectors – QWIP – T2SL – space systems

Contents

- 1 Introduction
- 2 Short History of Space-Based IR Telescopes
- 3 Fundamentals
- 4 Space Applications
- 5 Outlook
- 6 Conclusion

1. Introduction

Infrared (IR) detector technology has become essential for modern science and engineering. It is used ubiquitously from climate science to medical thermography and from agricultural monitoring to exodisk astronomy. (Rogalski 2011) In this essay I will first highlight the history of space-based IR telescopes. Then I will give an overview of the fundamentals of the physics of two new IR detector types, quantum well infrared photodetectors and type-II superlattice photodetectors, that are relevant for the later discussion of their application to asteroid and space debris detection. These two applications were selected because they highlight the advantages of the two detector types, specifically their radiation hardness, the wide range of regions in the IR they can be tuned to and their intrinsic suitability for sensing polarized light. Finally, I will present an outlook onto future developments for these two IR detector types.

2. Short History of Space-Based IR Telescopes

The history of space-based infrared detectors starts with the Infrared Astronomical Satellite (IRAS), launched in 1983 to perform the first survey of the night sky in IR using a 57cm aperture. (Neugebauer et al. 1984) Afterwards rapid development started, beginning with the launch of the Infrared Telescope, an 15cm aperture telescope, to the ISS in 1985. The Infrared Space Observatory launched in 1995, was the first telescope to detect the earliest stages of star formation with its 60 cm aperture. Both its instruments used SiGa detectors with a size of $32 \times 32 \text{ } 100\mu \times 100\mu$ pixels. (Boulade & Gallais 2000) Launched in 1996, the Mid-course Space Experiment was the next space telescope for the IR and was responsible for the only ever recorded incident of a person being hit by space debris. (Bartschi et al. 1996) The Spitzer Space Telescope, launched in 2003, flew two IR instruments: the Infrared Array Camera with multiple 256×256 -pixel

detectors and the Infrared Spectrograph with multiple 128×128 -pixel detectors, both using InSb and As-doped Si blocked impurity band technology. (Spitzer Science Center 2000) The following years saw many more IR detectors flown as part of diverse missions, most notable the Wide Field Camera 3 (WFC3) of the Hubble Space Telescope and the Herschel Space Observatory in 2009. The WFC3 is notable for its near-infrared HgCdTe array and whereas the Heterodyne Instrument for the Far Infrared from Herschel which was able to differentiate between two polarisations of the incoming light. (de Graauw et al. 2005) Also launched in 2009 the Wide-field Infrared Survey Explorer is responsible for discovering many of the asteroids discussed in subsection 4.1. (Wright et al. 2010) Currently, astronomers are looking to the James Webb Space Telescope for the next big IR telescope with Near InfraRed Camera (NIRCam), Near InfraRed Spectrograph (NIRSpec) and Mid-InfraRed Instrument (MIRI). MIRI has SiAs detectors with a resolution of 1024×1024 pixels. Wright et al. (2015)

3. Fundamentals

3.1. Physics of IR Photodetectors

Semiconductors can absorb photons when penetrated by a signal with enough photon power to generate photocarriers in the material. The signal decays exponentially as it travels through the semiconductor which can then be characterized with an absorption length α . For an ideal detector the responsivity R is

$$R = \frac{\lambda\eta}{hc}qG \quad (1)$$

with the quantum efficiency η , wavelength being λ and G the photoelectric gain. A useful parameter to compare detectors is their detectivity D^*

$$D^* = \frac{R(A_0\Delta f)^{1/2}}{I_n}, \quad (2)$$

which is their normalized signal-to-noise performance, where A_0 is its optical area, Δf is the frequency band and I_n is the noise current which is normally a combination of generation-recombination noise, Johnson noise and $1/f$ noise.

From Figure 1 it is clear that, additionally to the well known HgCdTe detectors, there are two other groups - Type-II Strained Layer Superlattice (T2SLS) and Quantum Dot Infrared Photodetectors (QDIP) - which offer high detectivity in the IR. In the following I will mostly focus on T2SLS and QDIP detectors due to their relatively recent consideration for space based IR detectors.

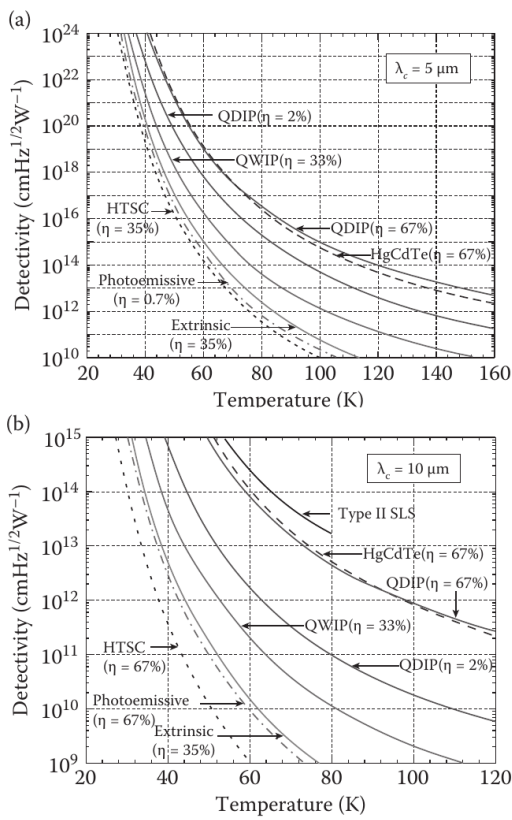


Fig. 1. Performance of different IR detectors. (Martyniuk & Rogalski 2008)

3.2. Physics of QWIPs

Quantum well infrared photodetectors (QWIP) and associated devices work through intersubband transition (ISBT), meaning the electron transition between confined (bound) states in quantum wells. Quantum wells for QWIPs are produced by growing layers of different semiconductor materials which produce heterojunctions in the detector (pixel) structure. (Schneider & Liu 2007) To produce stable structures the crystal properties of the two materials must be similar. A common choice is $Al_xGa_{1-x}As$ and $GaAs$ since the inclusion of Al impurity atoms have a negligible effect on the crystal structure and allows for tuning of the bandgap. (Rieke 2003) This detector structure results in the bandgap profile shown schematically in Figure 2 where the energies of the bands are roughly to-scale. The following discussion will focus on electrons as charge carriers, however the discussion is analogous for holes.

Conduction electrons near the quantum well can loose energy and "fall" into the lower energy states in the quantum well. The electrons will become trapped in this lower energy state and approximately behave according to the infinite potential barrier model. For cooled IR detectors this is generally a reasonable assumption, however it should be noted that in real, finite potential wells there is a finite number of allowed states. Additionally, the highest energy state(s) in finite potential wells can be at higher energies than the surrounding band and thus is a virtual state. Furthermore, for finite potential barriers, the trapped electrons have a finite probability to tunnel through thin potential barriers into adjacent quantum wells. If these wells are repeated and a bias voltage is applied to the detector pixel the band profile shown in Figure 3 develops. The detector can then transport electrons excited by incident photons to some collector. (Schnei-

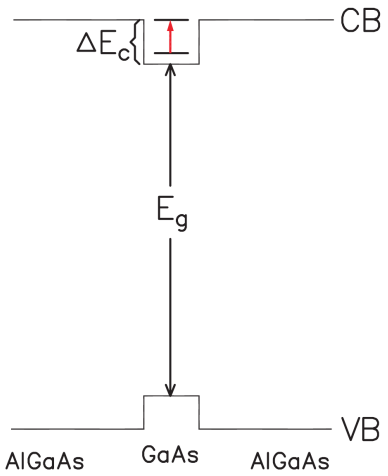


Fig. 2. Comparison of different IR detectors. (Schneider & Liu 2007, p.14)

der & Liu 2007) Real incident light is polarized in some plane, which poses an issue for the detectors which are grown in one direction. Assuming single band isotropic effective mass there is a selection rule as incident photons only excite electrons if they are polarized in the quantum well direction as shown by Levine et al. (1992); Schneider & Liu (2007). Liu et al. (1998) determined experimentally that this selection rule is generally accurate within 10%.

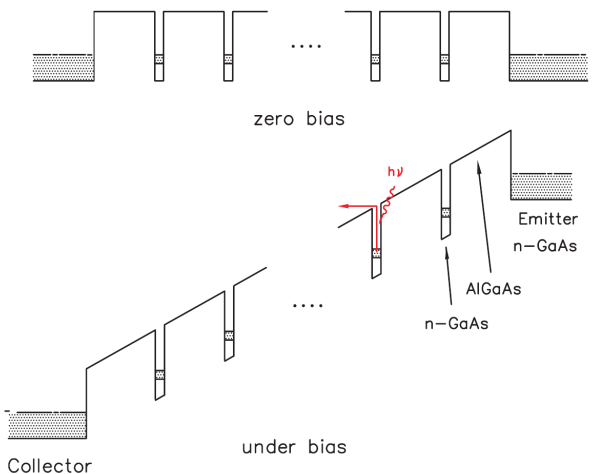


Fig. 3. Comparison of the energies required for interband and intersubband transition. The energies are shown roughly to-scale for $GaAs/AlGaAs$. (Schneider & Liu 2007)

Assuming both single band isotropic effective mass and an infinite potential barrier for a quantum well, the behaviour of the electrons inside it is described by the time-independent Schrödiner equation:

$$-\nabla \frac{\hbar^2}{2m*} \nabla \psi + V\psi = E\psi \quad (3)$$

with $m*$ the effective mass, V the potential of the well which has to have $V > E$ for it to be a well and with both V and E relative to some reference energy level. This formulation is generally valid no matter the dimension of the quantum well. By growing the semiconductors in specific structures it is also possible to create different quantum wells; bulk material allowing the electrons to move in 3 dimensions, the layered structure described

above gives allows the movement in two dimensions for an electron in a specific state (quantum well), an elongated tube allows movement in one dimension (quantum wire) and a cluster of differing semiconductor material spatially confines the movement of the electrons (zero-dimensional, quantum dot), see [Figure 4](#). The structure of the detector becomes macroscopic (negligible size quantization) on the scale of the de Broglie wavelength:

$$\lambda_{de\ Broglie} = \frac{h}{(2m^*E)^{1/2}} \quad (4)$$

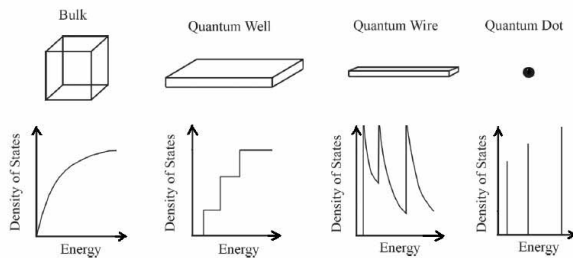


Fig. 4. Quantum wells in different with electron energies quantized in some axes. The density of states is not discrete due to the finite life time of the electrons in real materials. ([Xu et al. 2005](#))

For quantum wells the electrons occupy energy levels

$$E_n = \left(\frac{\hbar^2 \pi^2}{2m^* W^2} \right) n^2, \quad n = 1, 2, 3\dots \quad (5)$$

which is also their confinement energy in the dimension of W . W is the width of the quantum well, under the assumptions made above ($W = W_z \ll W_x, W_y$ and $W_x, W_y > \lambda_{de\ Broglie}$ i.e. electron energy is not quantized in 2 dimensions). For quantum wires and dots the electron energy is further quantized in other dimensions. This results in an increase in discretization of the total energy of the electron

$$E = E_n + E_m + E_l, \quad (6)$$

For the quantum well discussed above the equation would include the quantized term E_n from [Equation 5](#) in the axis of the quantum well and E_m, E_l as classical, non-quantized energies along the two perpendicular axes. For a fully confined electron (perfect quantum dot) the possible energy states are:

$$E^{0-D} = \frac{\hbar^2 k_{nx}^2}{2m^*} + \frac{\hbar^2 k_{my}^2}{2m^*} + \frac{\hbar^2 k_{lz}^2}{2m^*}, \quad n, m, l = 1, 2, 3\dots \quad (7)$$

where k is the momentum vector of the electron along the specified axis. The increasing discretization of the energy spectrum and density of states distribution with the decreasing degrees of freedom of the electron can be seen in [Figure 4](#). ([Choi 1997](#))

The total number of states in the quantum well is limited in reality due to the finite potential barrier of the well. For a given material and temperature the width of the quantum well determines the number of possible states. Well width increases the virtual states existing in the conduction band become possible in the well as can be seen in [Figure 5](#). The concentration of electrons n is then written as the product of the density of states $\rho(E)$ and the Fermi-Dirac distribution $f(E)$

$$n = \int \rho(E) f(E) dE \quad (8)$$

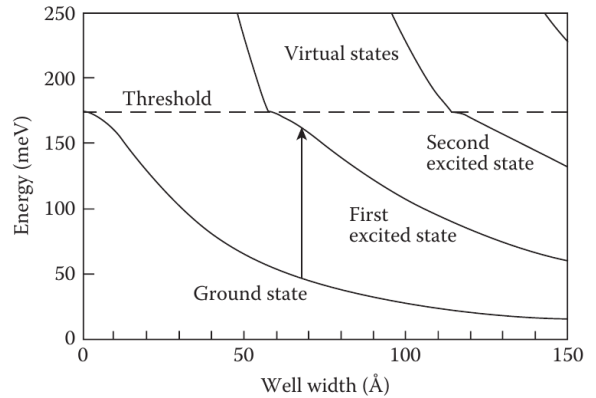


Fig. 5. Quantum well width and thresholds for the transition of virtual states to allowed states. ([Coon & Bandara 1991](#))

Detection of an incoming photon by a QWIP typically proceeds as follows; by applying a bias to the detector as shown in [Figure 3](#) the free electrons become trapped in the quantum wells until and an incoming photon of appropriate wavelength lifts an electron out of the quantum well into the conduction band (bound-to-continuum) of the detector in which it travels as photocurrent to the collector. For many QWIPs the incident photons cannot be normal to the structure due to the selection rule. In practice this poses an issue for QWIPs which can be solved through reflective gratings which scatter the incident photons or faceted detectors, see [subsection 3.4](#).

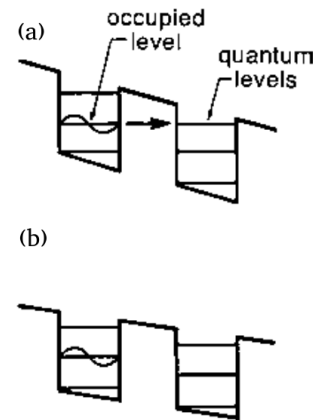


Fig. 6. Allowed transition (a) forbidden transition due to misaligned energy levels (b) for neighbouring quantum wells. ([Rieke 2003](#))

3.3. Physics of T2SL

Superlattice (SL) function on the same basics as QWIPs. In QWIPs each state in a quantum well forms a subband and, if many wells are placed next to each, these subbands form a minibands. This requires that a subband a quantum well corresponds to a subband of a neighbouring quantum well (see [Figure 7](#)). This effect is due to the penetration of the wave function into the finite potential barrier of the quantum wells mentioned above. The wave function penetrates the barrier where the probability drops exponentially. This exponential tail can overlap with empty allowed states in the adjacent quantum well if the permitted energy levels are aligned (see [Figure 6](#)), thus allowing quantum tunnel-

ing of the electron. The structure that is formed by the patterning of quantum wells and semiconductor layers is the SL. This allows for detection of photons which do not have enough energy to raise a trapped electron out of a quantum well into the conduction band. Instead it is sufficient if the electron is raised into a miniband through which the electron can travel to the collector as long as the energy levels are aligned. This is called a bound-to-bound transition. For biased superlattices this is process that occurs in steps as a cascade since the electron need to decay to a lower energy state before another bound-to-bound transition can occur (see [Figure 6](#)).

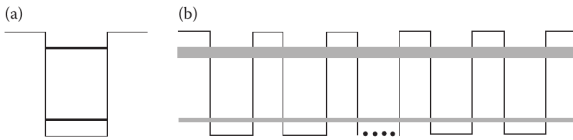


Fig. 7. Subbands (a) form minibands (b) when quantum wells are patterned and the wave functions for the allowed electron states overlap. ([Schneider & Liu 2007](#))

In general this bound-to-bound process can happen spontaneously even for ground-state electrons and hence detectors suffer from a large dark-current which cannot be reduced by cooling it. Furthermore, the spectral response of detectors employing bound-to-bound transitions is narrow since the photon induced transition is between moderate-width subbands. Hence detectors have largely focused on bound-to-continuum operation to avoid the issues with the bound-to-bound operating mode. Both modes require careful tuning of the alignment of the subbands of neighbouring quantum wells either to allow or inhibit bound-to-bound transmission. ([Rieke 2003](#))

The discussion in [subsection 3.2](#) mainly relates to superlattices which are composed of alternating layers from different semiconductors, however similar band profiles can also be formed by alternating n- and p-doped layers of a single semiconductor, which are called doping SL. Combinations of both types are also possible. ([Rogalski 2011](#))

There are four types of SL, three of which are shown in [Figure 8](#):

Type-I: For this type $\Delta E_c + \Delta E_v = E_{g2} - E_{g1}$ and all free charge carriers accumulate at one of the semiconductors. It is often used for injection lasers.

Type-II: There are two groups of Type-II SL (T2SL) based on whether the band gaps overlap and which both have $\Delta E_c - \Delta E_v = E_{g2} - E_{g1}$. This type will be discussed in more detail below.

staggered: For staggered T2SL the band gaps overlap and the electrons and holes accumulate at different semiconductors.

misaligned: For misaligned T2SL the conduction band of one semiconductor overlaps the valence band of the second one. The electrons enter the valence band of the second semiconductor and form a dipole layer together with the holes.

Type-III: This type consists of one semiconductor with a positive bandgap together with a semiconductor with a negative bandgap.

n-i-p-i structure: These SL consist of spatially modulated periodic n-doped, undoped¹, p-doped, undoped semiconductors which produce an effective band profile by having the

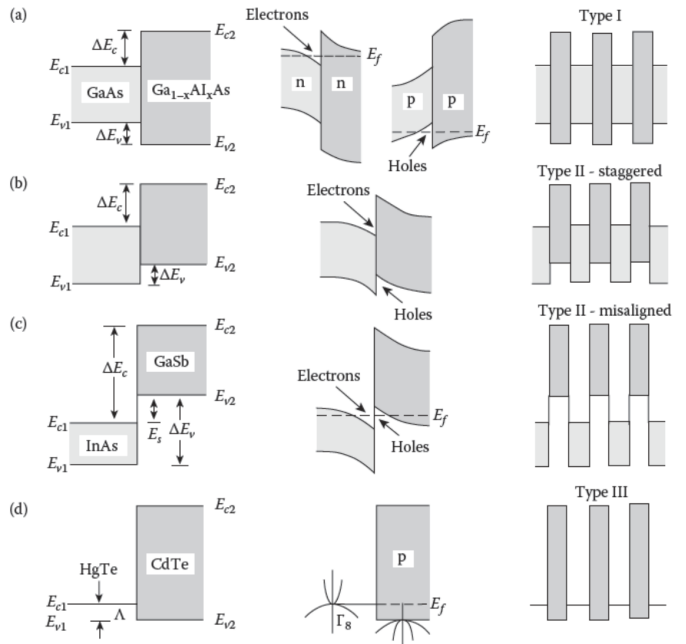


Fig. 8. band profiles and structure of different types of SL. ([Rogalski 2011](#))

potential oscillate between the n- and p-doped layers as is shown in [Figure 9](#). The effective bandgap E_g^{eff} is smaller than the actual bandgap of the intrinsic and doped semiconductor.

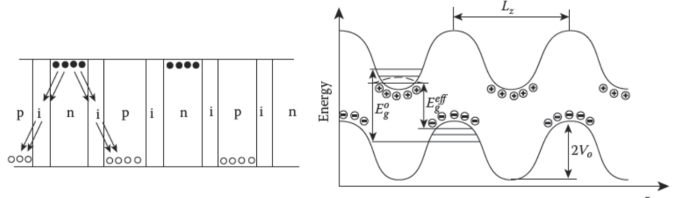


Fig. 9. Structure and schematic band profile with charge carrier traps for n-i-p-i structures. ([Rogalski 2011](#))

T2SL can be used for mid- and long wave photodetection through intersubband transition but also through transition from the valence to conduction band of neighbouring layers if the wave functions overlap sufficiently as is shown in [Figure 10](#). This is because, similar to n-i-p-i structures, the effective bandgap is reduced. Due to the transition between subbands in neighbouring layers absorption efficiency can be sufficiently high even with normal incidence photons.

Growing layers of slightly different semiconductors offers an opportunity to stress each layer due to a slight mismatches in their crystal structure. By growing layers with individually slightly varying lattice constants each layer is compression or tension loaded, resulting in an equal in-plane lattice constant. With sufficiently thin layers to avoid misfit defects this loading allows the tuning of the bandgap of the semiconductors. The effect of this loading is a significantly lower bandgap than can be achieved with any III-V alloy bulk photodetector. Most of these strained layer superlattice (SLS) detectors have moved to using InSb/InAsSb which rival the performance of HgCdTe detectors for IR detection.

¹ The "i" refers to intrinsic semiconductors, even though most of the n-i-p-i structures are based on GaAs

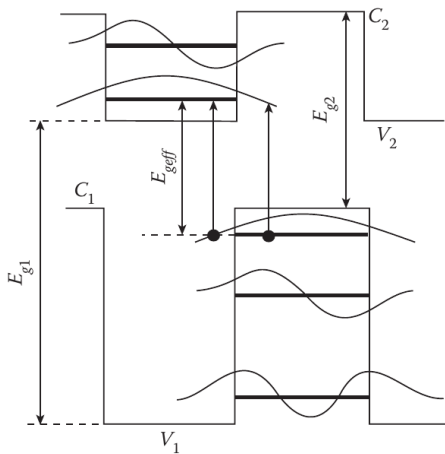


Fig. 10. Effective energy required for raising electrons out of the valence band of a T2SL (staggered). ([Rogalski 2011](#))

3.4. Materials & Production

One advantage of QWIPs and SL is that they can be produced from chemically stable, wide band-gap materials since they rely on inter-band excitation. Common materials are:

- GaAs/AlGaAs
- InGaAs/InAlAs
- InSb/InAsSb
- InAs/GaInSb
- SiGe/Si

Both QWIPs and T2SL(S) are produced using molecular beam epitaxy (MBE) which deposits thin-films of single crystals and is a mature technology for semiconductor manufacturing. ([Rogalski 2011](#); [Fastenau et al. 2001](#); [Bacher et al. 1997](#)) As shown in [Figure 11](#) MBE can grow large megapixel focal plane arrays of QWIPs and SL with a high yield and detector uniformity unlike what can be done for HgCdTe detectors. Single wafers can be grown up to 150mm are common today with 200mm and larger wafer also becoming possible recently. ([Forrai et al. 2007](#)) These focal plane arrays can be manufactured with the grating for polarimetric QWIPs directly applied to the structure. Similarly, as mentioned above the grating required to

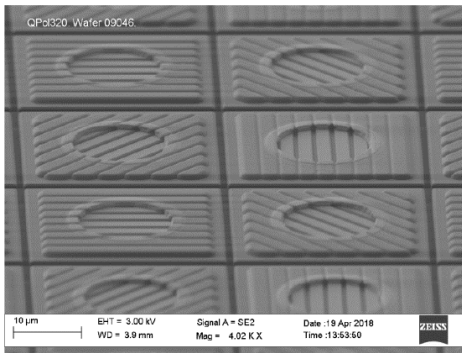


Fig. 11. Polarization grating in QWIP focal plane arrays from IRnova. ([Höglund 2021](#))

scatter normal incidence photons back into the detector pixel can also be directly implemented to the pixel structure as is shown in [Figure 12](#). QWIPs can also be grown as corrugated pixels so that either the layers themselves are angled to allow normal incidence light to excite electrons or so that the angled sides of the

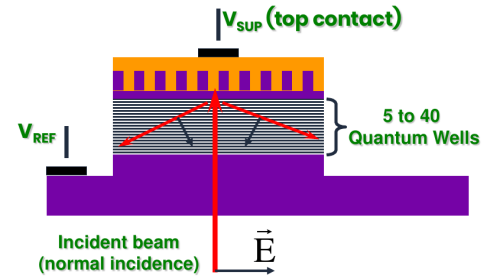


Fig. 12. Reflection grating and schematic structure of a QWIP. ([Höglund 2021](#))

pixel reflect the photons back into the material as is shown in [Figure 13](#). These corrugated pixels are typically etched into the

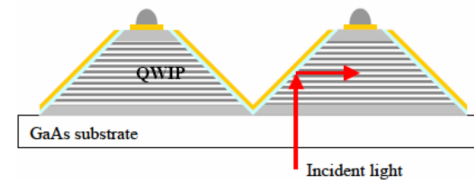


Fig. 13. Reflection of incidence light in corrugated QWIPs. ([Forrai et al. 2007](#))

grown layer structure and their main advantage is to reduce production cost. However, their quantum efficiency is limited due to the geometry of the structure which reduced the volume in which photons can interact with the quantum wells by 50%. ([Choi et al. 2005, 2007](#))

4. Space Applications

4.1. Asteroid Detection

Near earth asteroids (NEA) can pose a significant threat to humanity. Asteroids are typically considered potentially hazardous asteroids (PHA) if they are larger than 140m and their minimum orbit intersection distance with respect to Earth's orbit is below 0.05 AU. These asteroids, if impacting earth, are able to cause regional devastation through airbursts, earthquakes, tsunamis or direct impact on an unprecedented scale. Nevertheless, even smaller asteroids can cause significant damage if impacting near populated areas as can be seen in [Figure 14](#).

NASA currently estimates to have identified less than 40% of PHA with estimated diameters of above 140m ([Vereš et al. 2017](#)), however the detection completeness for PHA with a diameter larger than 10m is probably well be below 1% according to [Harris & Chodas \(2021\)](#) and [Schunová-Lilly et al. \(2017\)](#). Additionally, there is a need to detect PHAs far in advance, since most non-nuclear deflection strategies rely on multiple years (typically more than 10) of advanced warning. In order to improve the capabilities for planetary defense there is a clear need for new telescopes to increase survey completeness and lead time as can be seen in [Figure 15](#). IR detectors offer several advantages for asteroid detection and classification. The albedo of asteroids is very small, typically below 0.15, so visual detection is only possible for large and near objects, see [Figure 16](#). However, since most interesting asteroids have semi-major axes close to 1 AU their subsolar temperature is typically around 250 K which means that their emission spectrum peaks in the IR as can be seen from [Figure 18](#). ([Lim et al. 2005](#); [Mommert et al. 2018](#)) Fur-

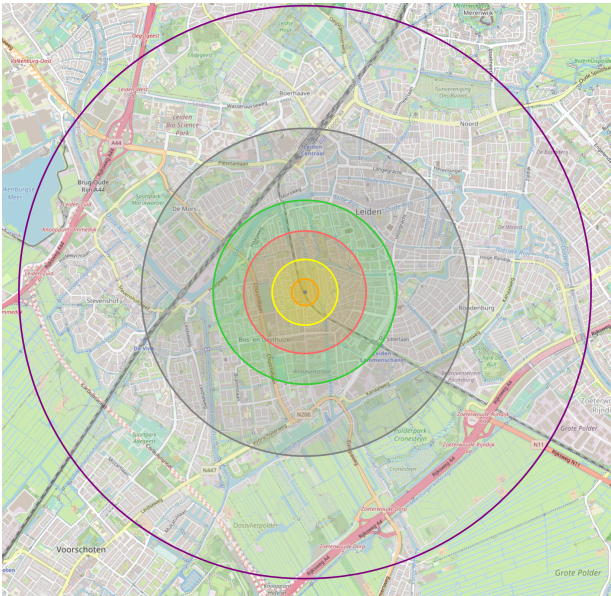


Fig. 14. PHA impact damage map for an PHA with 10m diameter without airburst (least severe scenario), centered on Leiden. Red: Probably fatal, Green: buildings destroyed. Image generated by McBurney (2020)

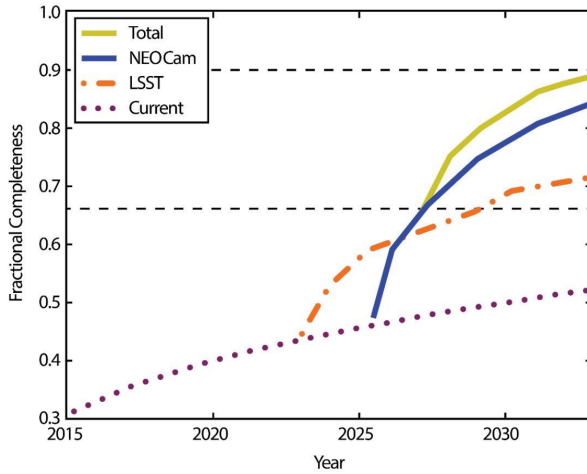


Fig. 15. NEA survey completeness for objects with a diameter larger than 140m. (Melosh et al. 2019)

thermore, the emissivity of NEA is very consistent at $\epsilon \approx 0.98$ according to Stokes et al. (2017). Hence, IR telescopes can differentiate between small but bright objects and large but dim objects whereas visible telescopes cannot. (Pravec et al. 2012; Masiero et al. 2021) In effect this reduces a source for biasing survey results. (Grav et al. 2011) Compoundingly this means that, with sufficient quality samples of NEAs space based IR telescopes can determine their diameter within 10–20% according to Mainzer et al. (2011a,b). Observations in the visible spectrum require a priori knowledge or estimation of the albedo of the asteroid which is correlated to its taxonomic type. (Thomas et al. 2011) This is a significant source of bias in the estimation of the NEO diameter and size which limits the usability of surveys in the visible spectrum (Melosh et al. 2019; Usui et al. 2014), especially since the spacecraft are roughly the same cost as ones with IR based telescopes according to Stokes et al. (2017). See Figure 17 for comparison of the basic flow in IR space-based and visible spectrum ground based NEA surveys.

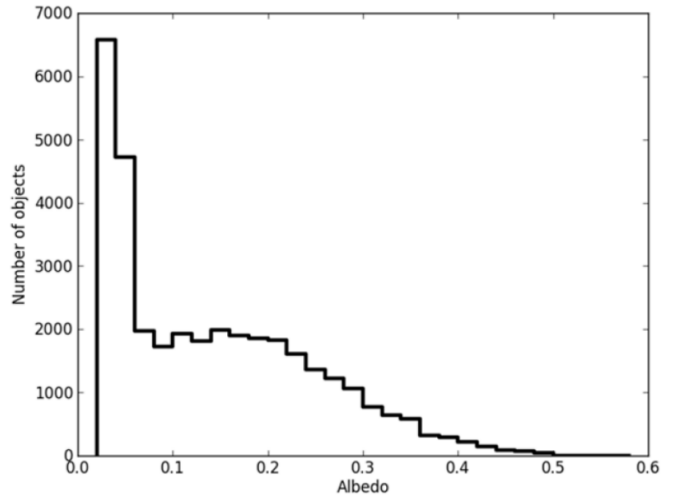


Fig. 16. NEA albedo distribution for objects with a diameter larger than 100m. (Stokes et al. 2017).

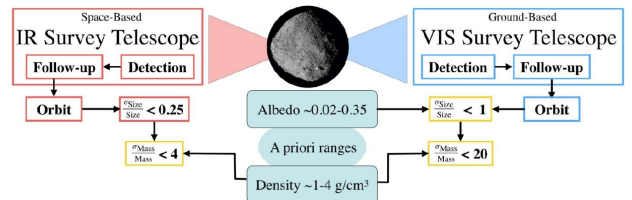


Fig. 17. Flow chart comparing the different approaches of best-case IR space based and visible spectrum (VIS) ground-based surveys. (Melosh et al. 2019)

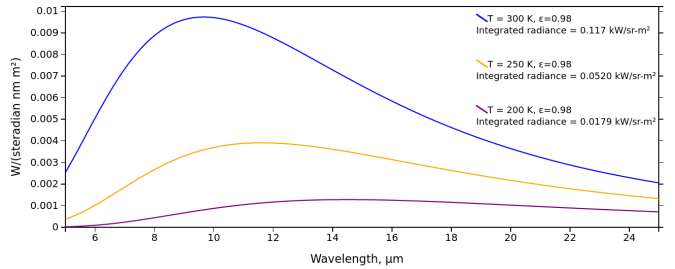


Fig. 18. Example of NEA emission spectrum in the IR with subsolar temperatures of 200 K (purple), 250 K (orange) and 300 K (blue). Asteroid properties are figures of merit taken from Lim et al. (2005).

For NEA detection interior to earth's orbit a space based telescope is needed since ground-based IR telescopes cannot observe in that direction. Detectors for space application need to be either protected from high energy radiation or be radiation hardened. QWIPs have intrinsic radiation hardness since the band gap of the Semiconductors (e.g. GaAs) can be large as inter-subband transition is used for photodetection. In practice this means that QWIPs are suitable for space-applications even when exposed high energy particles as shown first by Khanna et al. (1996) as well as Tidrow et al. (1999). Nevertheless, exposure to high energy proton and especially alpha radiation does degrade the detector over time due to their effect on the crystal structure. (Khanna et al. 1996) When exposing modern QWIPs to 20 Si hard particle radiation, equivalent to 63.3 MeV proton radiation (characteristic for space environments), no decrease of dark current, noise and responsivity was measured by Marshall

et al. (2009). Furthermore, they detected an increase in the percent of hot pixels of only 0.1% which was decreased by a factor of 10 after a room temperature anneal. This could be a strategy to heal QWIPs exposed to the space environment to re-set their performance through thermal control systems of the space-craft. T2SL suffer from the same issue which however more pronounced, especially for SLS due to the mechanical degradation of the structure when exposed to alpha particles. (Cowan et al. 2013; Jackson et al. 2010) Furthermore there is a significant decrease in the quantum efficiency for T2SLS when exposed to particle radiation as is visible in Figure 19. Again, annealing at room temperature restored a large part of the damage. (Cowan et al. 2012)

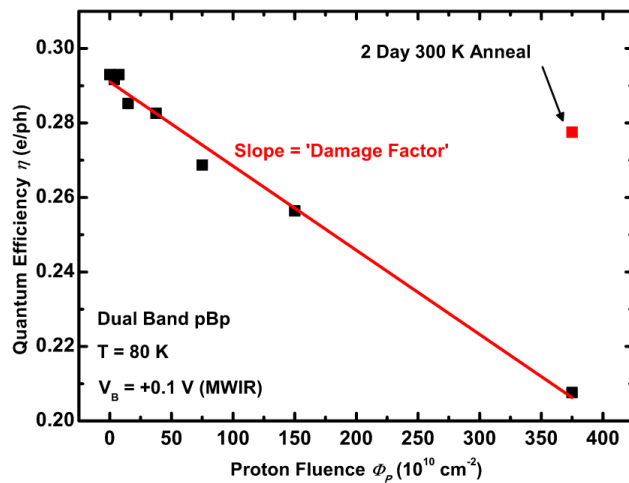


Fig. 19. Quantum efficiency degradation at $\lambda_p \sim 3.9\mu\text{m}$ of a dual band InAs/GaSb T2SLS pBp detector exposed to 63 MeV protons. (Cowan et al. 2012)

For both QWIPs and T2SL coatings can be used to increase radiation hardness which can be used up to long wave and multi color IR detectors/arrays. (Sood et al. 2006)

A significant advantage QWIP/QDIPs and T2SL(S) have over other IR detectors is their cost. The way both detectors are grown allows for low cost-high yield production of focal plane arrays as discussed in subsection 3.4. According to Melosh et al. (2019) and Stokes et al. (2017) small IR space based telescopes at L1 or L2 with an aperture of 0.5 m are well suited for NEO/PHA detection and tracking. A significant obstacle however is the cost of space based telescopes. Based on previous work by Stahl & Henrichs (2016) and Stokes et al. (2017) find that the cost of this 0.5m aperture IR telescope in space is roughly equivalent to a dedicated 8m visible light telescope at about \$480 million. This highlights the importance of scaled space systems for which can make use of inexpensive detectors. The systems analyzed by Stokes et al. (2017) make use of CCDs which result in a high cost for the scientific payload at roughly 48% of total system cost. This cost might be significantly reduced by using QWIP/QDIPs or T2SLS which have not been considered in the study.² This might enable multiple systems to be launched for a negligible increase in cost, especially for telescopes stationed in low earth orbits. (Stokes et al. 2017)

² Assuming other costs such as spacecraft structures etc. are constant when switching detectors.

4.2. Orbital Debris Detection

Orbital debris is a serious problem and many initiatives try to find ways to reduce the amount of space debris in low earth orbit and other crowded regions around earth. (Tolomeo et al. 2021; Andrenucci et al. 2011) Currently no dedicated space-based system exists to detect and/or classify space debris. Ground based telescopes track all known debris larger than 10cm, however smaller particles are still a high threat but too numerous and faint to be tracked reliably and cost-efficiently with existing telescopes. Space-based IR telescopes have been used to detect possible debris objects as small as 1 mm in size at a 1000 km distance. However, extrapolating these results to the general population very problematic due to the calibration of sensors. (Wesselius et al. 1993; Muntoni et al. 2017; Ahmed et al. 2019) When detecting space debris in the IR many of the above considerations for asteroids still apply. I would like to focus on an aspect not discussed for asteroids, polarization and polarimetric imaging of space debris. Generally, the space debris that is hazardous to operations is man-made. This means that the objects that are large enough to be detectable generally have geometric structures with either continuous curvatures or planes. This structure will be recognizable to detectors which can differentiate different polarization. When incoming unpolarized sunlight is reflected

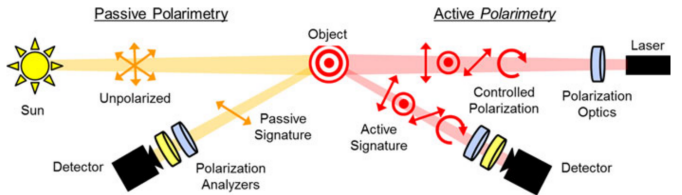


Fig. 20. Schematic measurement setup for detecting passive and active polarization of scattered light. (Pasqual & Cahoy 2017)

from space debris it becomes strongly polarized depending on the objects properties and the wavelength of the incoming light, see Figure 20. (Pang et al. 2017) As discussed in subsection 3.4 QWIPs and T2SL(S) are well suited for detecting the polarization of light reflected off objects. Hence, observing the scattered polarized light can provide the following information about the observed object:

- From photometry
 - distance to object
 - object shape
 - object size
- From polarization
 - object roughness
 - object material (estimate based on albedo)
 - object attitude
 - object shape
 - object motion (spin)

Ivanov et al. (2018) demonstrate that their QWIP focal plane arrays are able to image polarimetric signatures with integration times below 5 ms. This both highlights the readiness status of this technology but also shows a need for on-board pre-processing of the data to reach acceptable downlink data rates. (Larson & Wertz 2011) Using these IR detectors is useful for this application because of three main reasons. Firstly, the objects are typically brightest in the IR emission due to their temperature. While, unlike the NEA discussed in subsection 4.1, their albedo can be high when viewed from one or multiple orientations relying on this being the case biases the detection

and neglects some of the most common types of debris such as solid rocket motor particulates and carbon particles. (Mulrooney 2004; Krisko 2007) IR detectors will result in less biased surveys except for very cold objects. Nevertheless, these objects are typically very visible in the optical and are reliably tracked by ground based telescopes. (Muntoni et al. 2017) Secondly, the background brightness of space debris observed in IR is much lower than for optical observations. Özgün Yilmaz et al. (2019) Lastly, there are many proposed systems to deorbit space debris, one of the most effective and low-cost solutions is to decelerate small objects by irradiating them, either through direct impulse imparted by the incoming photons, through radiation pressure induced by heating the object or through sublimation of the material itself. (Fang et al. 2019; Choi & Pappa 2013) All methods would heat up the objects which will make it brighter in the IR and/or move the peak emission to the mid/near IR. Furthermore, using the polarization of light would allow these laser systems to determine more efficiently which objects to target and when to target them based on the information about the shape and surface properties that the polarized light provides.³

5. Outlook

One significant direction of development recently are multi-color detectors. QWIPs have multicolor capability, however read out circuits are limiting development. Several groups such as Caulfield (2003) are working on bio-inspired designs to overcome these issues. Both QDIPs and T2SL are well suited for further developments in that direction due to their production-side advantages over HgCdTe detectors. Rogalski (2011); Plis et al. (2015)

Naturally, the development of high-resolution detectors is a priority for astronomy. For further developments in that direction, advances need to be made both in the processing of the pixel data and the production methods of the focal plane arrays. Since many semiconductor devices rely on processes also used to create QWIPs and T2SL further progress seems likely. (Diel et al. 2018)

Cooling of detectors is a significant challenge, as can be seen from the troubled development of the James Webb Space Telescope. Hence, progress with Hot IR detectors seems like a promising path to lower the costs of space missions, especially for small cubesat based missions. Again, QWIPs and T2SL offer development paths. (Lyman & Krishnamoorthy 2020)

Very long wave infrared detectors are not only interesting for the applications discussed in this essay but also other astronomical science. Progress seems promising with devices related to QWIPs; Quantum cascade detectors, and further improvements of band profile manipulation could have important implications for both QWIPs and T2SL(s). (Liu et al. 2014; Plis et al. 2015)

Finally, the real deciding question will be if QWIPs and T2SL(S) will be able to compete with HgCdTe detectors in the future for large scientific missions. While both offer some advantages over the more mature and traditional detectors, their quantum efficiency is lower. (Rogalski 2011) The deciding factor here might not be the technical performance of the detectors but the cost related to their production and advancements in thin-film deposition technologies.

³ I have actually not seen this double synergy mentioned, neither in studies looking at telescopes for detecting and tracking objects nor in the studies of de-orbiting objects using lasers.

6. Conclusion

In this essay I give an overview of the basic physics of both QWIPs and T2SL and SLS. I relate the physics and the resulting detector properties to two space-based applications; detection of asteroids and detection of space debris. For the former, IR detectors in general and both QWIPs and T2SL(S) based telescopes would offer a significant and necessary addition to current capabilities. I identify the radiation hardness of QWIPs as an important aspect for the design of small scale space telescopes. For the detection of space debris, space-based IR telescopes fill the essential niche of detecting objects smaller than a few cm. The inherent ease of detecting the polarization of light with QWIPs is a significant advantage over other detector types. This would give laser systems for deorbiting space debris the ability to effectively choose targets for efficient operation. I identify the heating up of the targeted objects as a novel opportunity for synergy between these deorbiting systems and space-based object tracking IR telescopes. Finally, I give a short overview of promising developments in the field.

Acknowledgements. I would like to thank Dr. Leonard Burtscher for coordinating the inspiring lecture series as well as the different researchers and engineers for their talks. I would also like to thank Alexandra Elbakyan.

References

- Ahmed, R., Majurec, N., & De Bleser, J. w. 2019, in First International Orbital Debris Conference, Vol. 2109, 6079
- Andrenucci, M., Pergola, P., Ruggiero, A., Olympio, J., & Summerer, L. 2011, Active Removal of Space Debris Expanding foam application for active debris removal (European Space Agency (Advanced Concepts Team))
- Bacher, K., Massie, S., & Seaford, M. 1997, Journal of Crystal Growth, 175-176, 977, molecular Beam Epitaxy 1996
- Bartschi, B. Y., Morse, D. E., & Woolston, T. L. 1996, Johns Hopkins APL Technical Digest, 17, 215
- Boulade, O. & Gallais, P. 2000, Experimental Astronomy, 10, 227
- Caulfield, J. 2003, in 32nd Applied Imagery Pattern Recognition Workshop, 2003. Proceedings., 7–10
- Choi, K. K. 1997, Series in Modern Condensed Matter Physics, Vol. 7, The Physics of Quantum Well Infrared Photodetectors (World Scientific Publishing)
- Choi, K. K., Devitt, J. W., Forrai, D. P., et al. 2007, in Society of Photo-Optical Instrumentation Engineers (SPIE) Conference Series, Vol. 6542, Infrared Technology and Applications XXXIII, ed. B. F. Andresen, G. F. Fulop, & P. R. Norton, 65420S
- Choi, K. K., Monroy, C., Goldberg, A., et al. 2005, Infrared Physics and Technology, 47, 76
- Choi, S. H. & Pappa, R. S. 2013, Assessment Study of Small Space Debris Removal by Laser Satellites, Technical Report NASA/TP-20120009369, National Aeronautics and Space Administration (Langley Research Center)
- Coon, D. D. & Bandara, K. M. S. V. 1991, Physics of Thin Films (Academic Press)
- Cowan, V. M., Morath, C. P., Hubbs, J. E., et al. 2012, Applied Physics Letters, 101, 251108
- Cowan, V. M., Treider, L. A., Morath, C. P., et al. 2013, in Nanophotonics and Macrophotonics for Space Environments VII, ed. E. W. Taylor & D. A. Cardimona, Vol. 8876, International Society for Optics and Photonics (SPIE), 65 – 72
- de Graauw, T., Caux, E., Guesten, R., et al. 2005, in American Astronomical Society Meeting Abstracts, Vol. 207, American Astronomical Society Meeting Abstracts, 35.03
- Diel, W., Pozzi, M., Evans, D., et al. 2018, in Society of Photo-Optical Instrumentation Engineers (SPIE) Conference Series, Vol. 10624, Infrared Technology and Applications XLIV, 106241O
- Fang, Y., Pan, J., Luo, Y., & Li, C. 2019, Acta Astronautica, 165, 184
- Fastenau, J., Liu, W., Fang, X., et al. 2001, Infrared Physics & Technology, 42, 407
- Forrai, D. P., Choi, K.-K., & Devitt, J. W. 2007, in Society of Photo-Optical Instrumentation Engineers (SPIE) Conference Series, Vol. 6660, Society of Photo-Optical Instrumentation Engineers (SPIE) Conference Series, 666010
- Grav, T., Mainzer, A. K., Bauer, J., et al. 2011, The Astrophysical Journal, 742, 40

- Harris, A. W. & Chodas, P. W. 2021, *Icarus*, 365, 114452
- Höglund, L. 2021, lecture.
- Ivanov, R., Smuk, S., Hellström, S., et al. 2018, *Infrared Physics & Technology*, 95, 177
- Jackson, E., Aifer, E., Canedy, C., et al. 2010, *Journal of Electronic Materials* volume, 39, 852–856
- Khanna, S., Liu, H., Wilson, P., Li, L., & Buchanan, M. 1996, *IEEE Transactions on Nuclear Science*, 43, 3012
- Krisko, P. H. 2007, *Proceedings of the Institution of Mechanical Engineers, Part G: Journal of Aerospace Engineering*, 221, 975
- Larson, W. J. & Wertz, J. R. 2011, *Space Technology Library*, Vol. 8, *Space Mission Analysis and Design*, 3rd edn. (Microcosm)
- Levine, B. F., Zussman, A., Gunapala, S. D., et al. 1992, *Journal of Applied Physics*, 72, 4429
- Lim, L. F., McConnochie, T. H., Bell, J. F., & Hayward, T. L. 2005, *Icarus*, 173, 385
- Liu, H. C., Buchanan, M., & Wasilewski, Z. R. 1998, *Applied Physics Letters*, 72, 1682
- Liu, J. Q., Zhai, S. Q., Liu, F. Q., et al. 2014, in *2014 Conference on Optoelectronic and Microelectronic Materials Devices*, 127–129
- Lyman, J. E. & Krishnamoorthy, S. 2020, *Journal of Applied Physics*, 127, 173102
- Mainzer, A., Grav, T., Masiero, J., et al. 2011a, *The Astrophysical Journal*, 736, 100
- Mainzer, A., Grav, T., Masiero, J., et al. 2011b, *The Astrophysical Journal*, 737, L9
- Marshall, C., Foltz, R., Kan, E., et al. 2009, *Proton Radiation Evaluation of TIRS QWIP and Indigo 9808 Multiplexer*, Test Report D111908_TIRS-QWIP_Indigo-9808, Crocker Nuclear Laboratory (University of California)
- Martyniuk, P. & Rogalski, A. 2008, *Progress in Quantum Electronics*, 32, 89
- Masiero, J., Wright, E., & Mainzer, A. 2021, *The Planetary Science Journal*, 2
- McBurney, P. 2020, *Asteroid Damage Visualization Map*
- Melosh, J., Harris, A., Ida, B. L., et al. 2019, *Finding Hazardous Asteroids Using Infrared and Visible Wavelength Telescopes* (Washington, DC: The National Academies Press)
- Mommert, M., Jedicke, R., & Trilling, D. E. 2018, *The Astronomical Journal*, 155, 74
- Mulrooney, M. 2004, *An Assessment of the Role of Solid Rocket Motors in the Generation of Orbital Debris*, Technical Report NASA/TP-20070013536, National Aeronautics and Space Administration (Johnson Space Center)
- Muntoni, G., Schirru, L., Pisani, T., et al. 2017, *Electronics*, 6
- Neugebauer, G., Habing, H. J., van Duinen, R., et al. 1984, *ApJ*, 278, L1
- Pang, S., Wang, H., Lu, X., Shen, Y., & Pan, Y. 2017, in *Society of Photo-Optical Instrumentation Engineers (SPIE) Conference Series*, Vol. 10463, AOPC 2017: *Space Optics and Earth Imaging and Space Navigation*, ed. C. Nardell, S. Xue, & H. Yang, 104631B
- Pasqual, M. C. & Cahoy, K. L. 2017, *IEEE Transactions on Aerospace and Electronic Systems*, 53, 2706
- Plis, E., Myers, S., Ramirez, D., et al. 2015, *Infrared Physics & Technology*, 70, 93, proceedings of *International Conference on Quantum Structures Infrared Photodetectors*, 2014
- Pravec, P., Harris, A. W., Kušnírák, P., Galád, A., & Hornoch, K. 2012, *Icarus*, 221, 365
- Rieke, G. 2003, *Detection of Light - From the Ultraviolet to the Submillimeter*, 2nd edn. (Cambridge University Press)
- Rogalski, A. 2011, *Infrared detectors*, 2nd edn. (CRC Press Taylor & Francis Group)
- Schneider, H. & Liu, H. C. 2007, *Springer Series in Optical Sciences*, Vol. 126, *Quantum Well Infrared Photodetectors - Physics and Applications*, 1st edn. (Springer-Verlag Berlin Heidelberg)
- Schunová-Lilly, E., Jedicke, R., Vereš, P., Denneau, L., & Wainscoat, R. J. 2017, *Icarus*, 284, 114
- Sood, A. K., Puri, Y. R., Becker, L., et al. 2006, in *Infrared Technology and Applications XXXII*, ed. B. F. Andresen, G. F. Fulop, & P. R. Norton, Vol. 6206, International Society for Optics and Photonics (SPIE), 404 – 416
- Spitzer Science Center. 2000, *Spitzer Space Telescope, Observer's manual*, National Aeronautics and Space Administration (Langley Research Center)
- Stahl, H. P. & Henrichs, T. 2016, in *Society of Photo-Optical Instrumentation Engineers (SPIE) Conference Series*, Vol. 9911, *Modeling, Systems Engineering, and Project Management for Astronomy VI*, ed. G. Z. Angel & P. Dierickx, 99110L
- Stokes, G. H., Barbee, B. W., Bottke, W. F., et al. 2017, *Update to Determine the Feasibility of Enhancing the Search and Characterization of NEOs - Report of the Near-Earth Object Science Definition Team* (National Aeronautics and Space Administration)
- Thomas, C. A., Trilling, D. E., Emery, J. P., et al. 2011, *The Astronomical Journal*, 142, 85
- Tidrow, M. Z., Beck, W. A., III, W. W. C., et al. 1999, in *Photodetectors: Materials and Devices IV*, ed. G. J. Brown & M. Razeghi, Vol. 3629, International Society for Optics and Photonics (SPIE), 100 – 113
- Tolomeo, R., Colón, T., Collado, C., et al. 2021, *NASA's Efforts to Mitigate the Risks Posed by Orbital Debris* (National Aeronautics and Space Administration (Office of Inspector General))
- Usui, F., Hasegawa, S., Ishiguro, M., Müller, T. G., & Ootsubo, T. 2014, *PASJ*, 66, 56
- Vereš, P., Farnocchia, D., Chesley, S. R., & Chamberlin, A. B. 2017, *Icarus*, 296, 139
- Wesselius, P., van Hees, R., de Jonge, A., Roelfsema, P., & Viersen, B. 1993, *Advances in Space Research*, 13, 49
- Wright, E. L., Eisenhardt, P. R. M., Mainzer, A. K., et al. 2010, *AJ*, 140, 1868
- Wright, G. S., Wright, D., Goodson, G. B., et al. 2015, *PASP*, 127, 595
- Xu, Y., Meehan, K., Guido, L., et al. 2005, Phd thesis, Virginia Tech
- Özgün Yıldız, Aouf, N., Checa, E., Majewski, L., & Sanchez-Gestido, M. 2019, *Proceedings of the Institution of Mechanical Engineers, Part G: Journal of Aerospace Engineering*, 233, 811